

# Core Residue Replacements Cause Coiled-Coil Orientation Switching *in Vitro* and *in Vivo*: Structure–Function Correlations for Osmosensory Transporter ProP<sup>†</sup>

Yonit Tsatskis,<sup>‡,§,||</sup> Stanley C. Kwok,<sup>||,⊥</sup> Elisabeth Becker,<sup>‡</sup> Chad Gill,<sup>‡</sup> Michelle N. Smith,<sup>‡</sup> Robert A. B. Keates,<sup>‡</sup> Robert S. Hodges,<sup>⊥</sup> and Janet M. Wood<sup>\*,‡</sup>

Department of Molecular and Cellular Biology, University of Guelph, Guelph, ON N1G 2W1, Canada, and Department of Biochemistry and Molecular Genetics, University of Colorado Denver, School of Medicine, P.O. Box 6511, Mail Stop 8101, Aurora, Colorado 80045

Received September 5, 2007; Revised Manuscript Received November 2, 2007

**ABSTRACT:** Protein ProP acts as an osmosensory transporter in diverse bacteria. C-Terminal residues 468–497 of *Escherichia coli* ProP (ProPEc) form a four-heptad homodimeric  $\alpha$ -helical coiled coil. Arg 488, at a core heptad *a* position, causes it to assume an antiparallel orientation. Arg in the hydrophobic core of coiled coils is destabilizing, but Arg 488 forms stabilizing interstrand salt bridges with Asp 475 and Asp 478. Mutation R488I destabilizes the coiled coil and elevates the osmotic pressure at which ProPEc activates. It may switch the coiled-coil orientation to parallel by eliminating the salt bridges and increasing the hydrophobicity of the core. In this study, mutations D475A and D478A, which disrupt the salt bridges without increasing the hydrophobicity of the coiled-coil core, had the expected modest impacts on the osmotic activation of ProPEc. The five-heptad coiled coil of *Agrobacterium tumefaciens* ProP (ProPA<sub>t</sub>) has K498 and R505 at *a* positions. Mutation K498I had little effect on the osmotic activation of ProPA<sub>t</sub>, and ProPA<sub>t</sub>-R505I was activated only at high osmotic pressure; on the other hand, the double mutant was refractory to osmotic activation. Both a synthetic peptide corresponding to ProPA<sub>t</sub> residues 478–516 and its K498I variant maintained the antiparallel orientation. The single R505I substitution created an unstable coiled coil with little orientation preference. Double mutation K498I/R505I switched the alignment, creating a stable parallel coiled coil. *In vivo* cross-linking showed that the C-termini of ProPA<sub>t</sub> and ProPA<sub>t</sub>-K498I/R505I were antiparallel and parallel, respectively. Thus, the antiparallel orientation of the ProP coiled coil is contingent on Arg in the hydrophobic core and interchain salt bridges. Two key amino acid replacements can convert it to a stable parallel structure, *in vitro* and *in vivo*. An intermolecular antiparallel coiled coil, present on only some orthologues, lowers the osmotic pressure required to activate ProP. Formation of a parallel coiled coil renders ProP inactive.

Changes in extracellular osmotic pressure disrupt cell structure and function by eliciting transmembrane water fluxes that concentrate or dilute the cytoplasm. Cells respond by adjusting the distributions of selected solutes across the cytoplasmic membrane, and water follows, restoring cellular hydration and volume (1). Multiple osmoregulatory systems adjust cellular solute content in response to osmotic stress (1, 2). The ProP protein of *Escherichia coli* (ProPEc) is denoted an “osmosensory transporter” because it senses increasing osmotic pressure ( $\Pi$ ) and responds by mediating

the cytoplasmic accumulation of organic osmolytes (3) both in intact cells and after purification and reconstitution into proteoliposomes (4). ProP is a member of the major facilitator superfamily (MFS)<sup>1</sup> (5) and a H<sup>+</sup>-solute symporter (6, 7). The structure of ProPEc is being elucidated (Figure 1A), and experimental data support a homology model for its membrane-integral helix bundles (8–10). ProP orthologues are divided into two classes based on the sequences of their cytoplasmic C-termini (10, 11). ProPEc and other group A orthologues terminate in series of heptad repeats characteristic of  $\alpha$ -helical coiled coils (Figure 1C). Group

<sup>†</sup> This work was supported by Natural Sciences and Engineering Research Council of Canada (NSERC) Discovery Grant OPG0000508 (J.M.W.), NIH Grant PO1AI059576 and the John Stewart Chair in Peptide Chemistry (R.S.H.), a NSERC PGSB Postgraduate Scholarship (M.N.S.), a NSERC Undergraduate Student Research Award (C.G.), and an award from the Hans Mühlenhoff Stiftung (E.B.).

<sup>\*</sup> To whom correspondence should be addressed: Department of Molecular and Cellular Biology, University of Guelph, Room 4251 Science Complex, 488 Gordon St., Guelph, ON N1G 2W1, Canada. Telephone: (519) 824-4120, ext. 53866. Fax: (519) 837-1802. E-mail: jwood@uoguelph.ca.

<sup>‡</sup> University of Guelph.

<sup>§</sup> Present address: Samuel Lunenfeld Research Institute, Toronto, ON M5G 1X5, Canada.

<sup>||</sup> These authors contributed equally to this work.

<sup>⊥</sup> University of Colorado Denver, School of Medicine.

<sup>1</sup> Abbreviations:  $\Pi$ , osmotic pressure;  $\Pi/RT$ , osmolality; ABC, ATP-binding cassette; BCA, bicinechonic acid; CD, circular dichroism; DTME, dithiobis(maleimidoethane); DTT, dithiothreitol; EDTA, ethylenediaminetetraacetic acid; EPR, electron paramagnetic resonance; FMOC, 9-fluorenylmethoxycarbonyl; HPLC, high-performance liquid chromatography; LB, Luria Bertani; MFS, major facilitator superfamily; MOPS, 4-morpholinopropanesulfonic acid; MW, molecular weight; NMR, nuclear magnetic resonance; OD, optical density; ORF, open reading frame; PCR, polymerase chain reaction; PDB, Protein Data Bank; RPC, reversed-phase chromatography; SDS–PAGE, sodium dodecyl sulfate–polyacrylamide gel electrophoresis; TFA, trifluoroacetic acid; TFE, trifluoroethanol; TIS, triisopropylsilane; *T*<sub>m</sub>, temperature at the midpoint of a thermal transition; TM, transmembrane segment; WT, wild type.

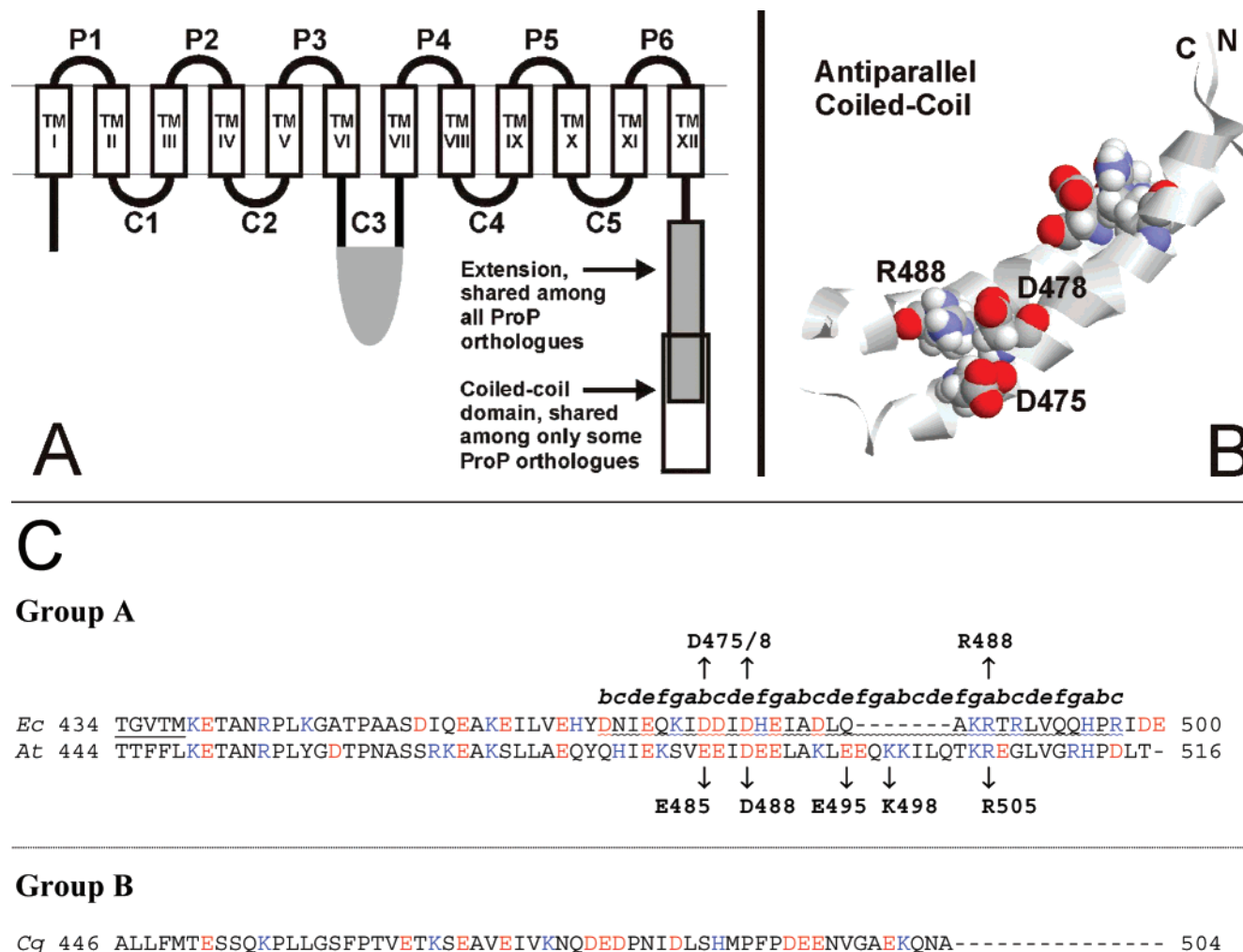


**FIGURE 1: C-Terminal domain of ProP.** (A) A member of the major facilitator superfamily, ProP, has 12 transmembrane helices (TMI–TMXII), six periplasmic loops (P1–P6), and five cytoplasmic loops (C1–C5) (9). The structures represented in black and white (not gray) were modeled with the crystal structure of paralogue GlpT as a template (9) (TMI–TMXII) or determined by NMR spectroscopy of the corresponding synthetic peptide (18) (the C-terminal coiled-coil domain, represented by the white box and shown in panel B). All ProP orthologues have extended C-termini (gray and white boxes). Only group A orthologues [including those from *E. coli* (ProPEc) and *A. tumefaciens* (ProPAtr)] share the C-terminal coiled coil (white box), and the coiled coil is absent from group B orthologues like that from *C. glutamicum* (ProPCg, gray box). (B) NMR solution structure of a peptide replica of residues D468–R497 of ProPEc (18). The antiparallel  $\alpha$ -helical coiled-coil structure appears to be stabilized by two salt bridges, each formed by the interaction of R488 on one strand with D475 and D478 on the other. (C) Alignment of the C-termini of ProPEc, ProPAtr, and ProPCg. Residues TGVTM of TMXII in ProPEc (underlined) are integral to the membrane (10). Residues D468–R497 of ProPEc (squiggly underline) are represented by the NMR structure in panel B (18). Letters *a–g* mark the coiled-coil heptad positions. Letters designating acidic residues are colored red and those designating basic residues blue. Upward-pointing arrows mark the positions of residues D475, D478, and R488 in ProPEc, and downward-pointing arrows mark the positions of residues E485, D488, E495, K498, and R505 in ProPAtr (see the text). Note that group B orthologue ProPCg shares an extended, anionic C-terminus with the group A orthologues but lacks the distal, basic sequence required for the coiled coil.

B orthologues have shorter C-terminal extensions with no heptad repeats (11).

Coiled-coil sequences are characterized by seven-residue heptad repeats with hydrophobic residues at core *a* and *d* positions. The polypeptide chains can associate with either parallel or antiparallel orientations. Residues at like positions are paired in the hydrophobic core of two-stranded parallel coiled coils (*a* with *a'* and *d* with *d'*). Residues at positions *e* and *g* may form interhelical ion pairs that increase stability and direct chain registry, but they can contribute an order of magnitude less to stability than the hydrophobic core (12–14). Core residues at unlike positions are paired in two-stranded antiparallel coiled coils (*a* with *d'* and *d* with *a'*), and ionic interactions can involve pairing of positions *e* with *e'* and *g* with *g'*. The packing of hydrophobes contributes

more to stability in the antiparallel than in the parallel orientation (15, 16). The interactions that maintain parallel, homodimeric coiled coils are relatively well understood (17). In contrast, orientation-specifying interactions for antiparallel coiled coils are less understood and may not be obvious from amino acid sequences (18–24). We investigated the determinants of orientation for the ProP coiled coil and elucidated the role of orientation in its biological function.

Parallel and antiparallel alignments for the four-heptad repeats of ProPEc (residues 468–497) are shown in panels A and B of Figure 2. The corresponding peptide formed a homodimeric  $\alpha$ -helical coiled coil, but it was unexpectedly disrupted when Arg 488 (in a heptad *a* position) was replaced with Ile (25). The nuclear magnetic resonance (NMR) structure of this peptide revealed a homodimeric antiparallel

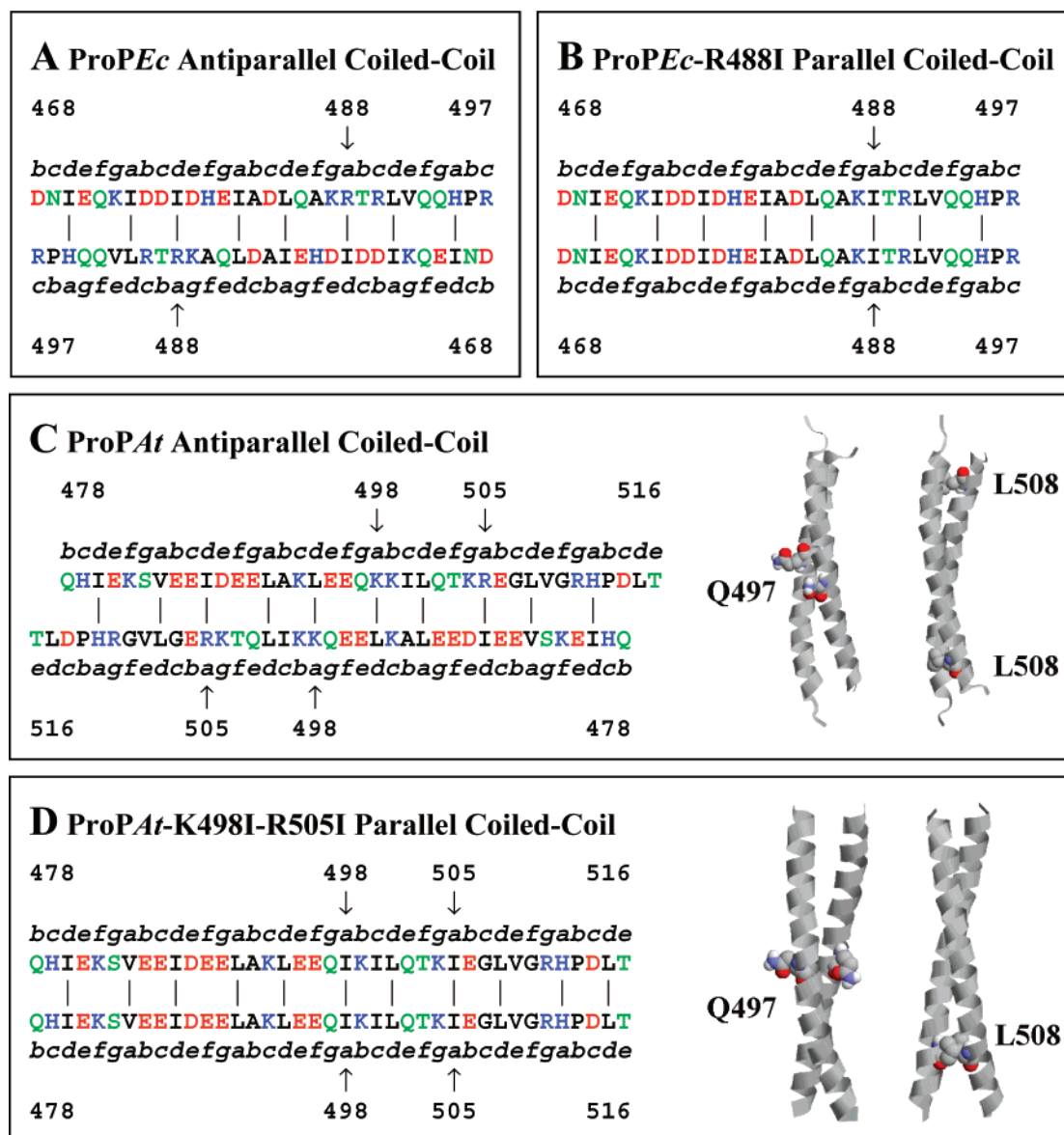


FIGURE 2: Homodimeric  $\alpha$ -helical coiled coils formed by the ProP C-terminal domains. (A) The sequence of ProPEc residues 468–497 is shown in the antiparallel alignment shown by the NMR structure of Zoetewey et al. (18) (see Figure 1B). (B) The sequence of ProPEc-R488I residues 468–497 is shown in the predicted, parallel alignment (27). (C and D) The sequences of ProPAtr and ProPAtr-K498I/R505I residues 478–516 are shown in the predicted antiparallel and parallel alignments, respectively. Letters a–g mark the coiled-coil heptads. In the antiparallel alignment, K498 is salt bridged to E495' and R505 to E485' and D488'. In each case, a structural model for the putative coiled coil is also shown (gray ribbons). Residues replaced with cysteine for cross-linking analysis during this study are highlighted. Q497 residues (g position) are proximal in both antiparallel and parallel orientations, whereas L508 residues (d position) are distal in the antiparallel orientation and proximal in the parallel orientation. Models were built using SPDBV (52). The antiparallel ProPAtr model was derived by extending the helices of the ProPEc structure (PDB entry 1R48) by seven residues and substituting the sequence of ProPAtr. The parallel model for ProPAtr-K498I/R505I was derived from the parallel coiled-coil structure 1ZXA [coiled-coil domain of cGMP protein kinase (53)]. Potential disulfide bond sites were tested in both models by making Cys substitutions in SPDBV and checking for a lack of disruptive effects on coiled-coil structure as well as appropriate S–S bond distance and orientation.

coiled coil (18). Arg in the hydrophobic core of parallel coiled coils is destabilizing because of electrostatic repulsion (12, 13), so pairing of Arg with Ile in the antiparallel orientation (Figure 2A) would be greatly favored over pairing of Arg with Arg in a parallel coiled coil. Interhelical salt bridges linking Arg 488 with Asp 475 and Asp 478 would offset the destabilizing effect of Arg in the hydrophobic core (Figures 1B and 2A). The NMR structure and other observations provided a rationale for the antiparallel orientation of this coiled coil and its disruption by replacement R488I (25, 26). While this mutation would eliminate the interhelical salt bridges that stabilize the antiparallel orientation, it would

also increase the continuous array of hydrophobic Ile and Leu residues, paired across the hydrophobic core, from only two in the antiparallel structure with Arg 488 to seven in the parallel structure with Ile 488 (Figure 2A,B).

There is also evidence that ProPEc dimerizes and antiparallel coiled-coil structures are present *in vivo*. When the transporter was expressed at a physiological level, Cys introduced in transmembrane segment (TM) XII or at coiled-coil position 480 could be cross-linked. Cys at other positions, including coiled-coil position 473, could not (10, 27). Residues at position 473 would be close in parallel, but not in antiparallel, coiled-coil dimers. The R488I mutation



impaired cross-linking of the 480C variant and enhanced cross-linking of the 473C variant, suggesting that antiparallel coiled coils are present in WT transporter dimers and the C-termini of R488I variants can be parallel (10).

More importantly, these structural phenomena have functional correlates. The group B ProP orthologue from *Corynebacterium glutamicum*, lacking the coiled coil, is activated at a higher osmolality than group A orthologues, which terminate in heptad repeats (11). Similarly, ProPEc variants with truncated C-termini and variant ProPEc-R488I are activated at much higher osmolalities than WT ProPEc (11). Thus, the coiled coil is not an osmosensor, *per se*, but it adjusts the response of group A transporters to a lower osmolality range. In addition to ProP, two other bacterial transporters are serving as model systems for the study of osmosensing: Na<sup>+</sup>-betaine symporter BetP and ATP binding cassette transporter OpuA. All three proteins are regulated by cytoplasmic, C-terminal extensions; however, the extensions are structurally unrelated, and the cytoplasmic domains of BetP and OpuA are believed to serve as osmosensing switches (1).

The R488I substitution in ProPEc has additional functional consequences that are helping us to understand how the coiled coil adjusts the transporter's response range. The activation of ProPEc is sustained, the activity remaining high as long as *E. coli* cells remain in high-osmolality medium. In contrast, osmotic activation of ProPEc-R488I is transient. ProPEc-R488I activity can be detected immediately after bacteria are subjected to an osmotic upshock, but that activity declines 10-fold within 1 h (25). Here we show that disrupting the coiled-coil salt bridges (mutations D475A and D478A) had a much weaker impact on ProPEc function than both disrupting the salt bridges and increasing the hydrophobicity of the coiled-coil core (single mutation R488I). Most importantly, the Asp to Ala replacements did not render ProPEc activation transient.

The group A ProP orthologue from *Agrobacterium tumefaciens* (ProPA<sub>t</sub>) includes five C-terminal heptads [as contrasted with four for ProPEc (Figure 1C)]. The antiparallel coiled coil of ProPA<sub>t</sub>, modeled on the *E. coli* structure, would have a total of four (rather than two) sets of salt bridges involving two basic residues in *a* positions (Figure 2C). In this work, we exploited the potential for modulation of ProPA<sub>t</sub> coiled-coil stability to explore the determinants of coiled-coil orientation and the relationship between coiled-coil structure and ProP function. Our data show that replacement of both core basic residues with Ile is necessary and sufficient to switch coiled-coil orientation and render ProPA<sub>t</sub> refractory to osmotic activation.

## EXPERIMENTAL PROCEDURES

**Peptide Synthesis, Oxidation, Purification, and Characterization.** Polypeptides were synthesized via a manual solid-phase methodology using 9-fluorenylmethoxycarbonyl chemistry (Fmoc). Manual solid-phase methodology has been described previously (28, 29). Different side chain protection groups Trt (trityl) and AcM (acetamidomethyl) were used to protect the N-terminal and the C-terminal Cys, respectively. This differential protection scheme allowed the formation of in-register parallel homo-stranded molecules linked at either the N- or C-termini with a disulfide bond.

For each peptide, this yielded two pairs of covalently linked homo-stranded molecules with matching sequences but with disulfide bridges at opposite ends. In addition, antiparallel hetero-stranded molecules linked at opposite ends could be generated by mixing the parallel molecules in REDOX reactions. When the N-terminal disulfide-bridged homo-stranded molecules were formed, the C-terminal cysteine was left protected with the ACM group. Crude polypeptides were purified by reversed-phase chromatography (RPC) on a Zorbax semipreparative SB-C8 column [9.4 mm (inside diameter) × 250 mm, 5 μm particle size, 300 Å pore size] by linear AB gradient elution (acetonitrile increasing 0.1%/min), where eluent A was 0.05% aqueous TFA and eluent B was 0.05% TFA in acetonitrile, at room temperature with a constant flow rate of 2 mL/min. The purity and homogeneity of the polypeptide were verified by analytical RPC on a Zorbax analytical SB-C8 column [4.6 mm (inside diameter) × 250 mm, 5 μm particle size, 300 Å], by quantitative amino acid analysis (Beckman model 6300 amino acid analyzer) and by electrospray mass spectroscopy using a Mariner Biospectrometry Workstation mass spectrometer (PerSeptive Biosystems, Framingham, MA). Sedimentation equilibrium analyses were performed as previously described (30). Peptide molecular weights and sedimentation behavior are reported as Supporting Information (Table S1).

**Circular Dichroism (CD) Spectroscopy.** CD spectroscopy was performed on a Jasco-810 spectropolarimeter with constant N<sub>2</sub> flushing (Jasco, Inc., Easton, MD), and the methodology was described previously (28, 30). For CD wavelength scans, a 5 mg/mL stock solution of each polypeptide in 100 mM potassium chloride and 50 mM potassium phosphate (pH 7) (benign solvent) was diluted into the same buffer to a concentration of 50 μM and scanned in the presence of 0.2 mM DTT and the presence and absence of 50% trifluoroethanol (TFE). Mean residue ellipticity [Θ] was calculated using the following equation:

$$[\Theta] = (\Theta_{\text{obs}} \text{mrw}) / (10lc) \quad (1)$$

where Θ<sub>obs</sub> is the observed ellipticity in millidegrees, mrw is the mean residue molecular weight, *l* is the optical path length of the CD cell (centimeters), and *c* is the polypeptide concentration (milligrams per milliliter). For thermal melting experiments, data points were taken at 1 °C intervals at a scan rate of 60 °C/h from 5 to 95 °C. *T<sub>m</sub>* was determined from a plot of fraction folded against temperature on the basis of the assumption that each peptide was fully folded at 5 °C and fully unfolded at 95 °C.

**REDOX Analyses by RPC.** The short and long versions of each peptide (defined in Results) were first individually disulfide-bridged and then stirred into a redox buffer to promote disulfide interchange. The short peptides were disulfide-bridged by stirring them in an iodine solution (100 mM in 30% aqueous acetic acid) under constant N<sub>2</sub> to remove AcM protecting groups from the C-terminal Cys and simultaneously oxidize them. The long peptides were disulfide-bridged by air oxidation of the unprotected N-terminal Cys [overnight stirring in a 100 mM NH<sub>4</sub>HCO<sub>3</sub> buffer (pH 8.5)]. The desired products were purified by RPC (described above). The short and long oxidized peptides were then mixed in a 1:1 ratio in the redox buffer [10-fold molar excess of reduced and oxidized glutathione (500 mM) in 100 mM

Table 1: Plasmids<sup>a</sup>

plasmid	encoded protein	source or reference
pBAD24	Nil (expression vector)	33
pDC79	ProPec	25
pDC80	ProPec-His <sub>6</sub>	39
pDC86	ProPec-R488I	25
pDC141	ProPec*-E480C	27
pYT15	ProPec-D475A	derived from pDC79
pYT16	ProPec-D478A	derived from pDC79
pYT17	ProPec-D475A/D478A	derived from pDC79
pYT18	ProPec-D476A	derived from pDC79
pYT19	ProPec-D475A/D476A/D478A	derived from pDC79
pYT13	ProPat	11
pCG1	ProPat-K498I	derived from pYT13
pYT14	ProPat-R505I	derived from pYT13
pCG2	ProPat-K498I/R505I	derived from pYT13
pEB1	ProPat-His <sub>6</sub>	derived from pYT13
pEB2	ProPat-K498I/R505I-His <sub>6</sub>	derived from pCG2
pEB3	ProPat-R505I-His <sub>6</sub>	derived from pYT14
pEB4	ProPat-K498I-His <sub>6</sub>	derived from pCG1
pEB5	ProPat-Q497C-His <sub>6</sub>	derived from pEB1
pEB6	ProPat-L508C-His <sub>6</sub>	derived from pEB1
pEB7	ProPat-Q497C/K498I/R505I-His <sub>6</sub>	derived from pEB2
pEB8	ProPat-K498I/R505I/L508C-His <sub>6</sub>	derived from pEB2

<sup>a</sup> Plasmids (except pBAD24) are pBAD24 derivatives containing fragments approximately 1.6 kb in size that encode ProPec, ProPat, or a variant of either transporter. *E. coli* ProP is denoted ProPec; a cysteine-less, histidine-tagged ProPec variant is denoted ProPec\*, and *A. tumefaciens* ProP is denoted ProPat.

KCl and 50 mM potassium phosphate (pH 8.0)]. At intervals, 5  $\mu$ L aliquots were taken and the reaction was quenched by adding 5% aqueous acetic acid (5  $\mu$ L). The reaction mixture was then separated by RPC on a Zorbax analytical SB-C8 column [4.6 mm (inside diameter)  $\times$  250 mm, 5  $\mu$ m particle size, 300 Å] using a slow gradient (0.33% acetonitrile/min) to measure the proportions of disulfide-bridged peptides that were homo-stranded (starting material) and hetero-stranded (new product).

**Culture Media.** *E. coli* strains were grown at 37 °C in LB medium (31) or in NaCl-free MOPS medium, a variant of the MOPS medium described by Neidhardt et al. (32) from which NaCl was omitted. MOPS medium was supplemented with NH<sub>4</sub>Cl (9.5 mM) as a nitrogen source and glycerol (0.4%, v/v) as a carbon source. L-Tryptophan (245  $\mu$ M) and thiamine hydrochloride (1  $\mu$ g/mL) were added to meet auxotrophic requirements. Ampicillin (100  $\mu$ g/mL) was included to maintain plasmids, and D-arabinose was added as specified to adjust *proP* expression.

**Bacteria, Plasmids, and Molecular Biological Manipulations.** Genes encoding ProP and its variants were expressed from the AraC-controlled P<sub>BAD</sub> promoter in plasmid-bearing derivatives of *E. coli* WG350 [F<sup>-</sup> *trp lacZ rpsL thi*  $\Delta$ (*putPA*)-101  $\Delta$ (*proU*)600  $\Delta$ (*proP-melAB*)212] (5). Each strain contained pBAD24 (33), or a pBAD24 derivative listed in Table 1. Basic molecular biological techniques were as described by Sambrook and Russell (34). Chromosomal DNA was isolated as described by Bayliss et al. (35). The polymerase chain reaction (PCR) was carried out as described by Brown and Wood (36). Site-directed mutagenesis was performed using the QuikChange mutagenesis kit (Stratagene, La Jolla, CA) as described by Culham et al. (8). Oligonucleotides were purchased from Cortec DNA Services (Kingston, ON). Each recombinant plasmid was recovered from a ligation mixture by transformation of *E. coli* DH5 $\alpha$  (37), and the entire sequence of the encoded *proP* variant was confirmed

(GenAlyTiC, Guelph, ON) before the plasmid was expressed in *E. coli* WG350.

**Transport Assays.** Bacteria were cultivated and assays performed as described by Culham et al. (38) using the media described above and buffers prepared as described by Racher et al. (39). Osmolalities of culture media and buffers were adjusted with NaCl and measured with a Wescor vapor-pressure osmometer (Wescor, Logan, UT). With the pBAD vector system, variations in expression of transporter variants can be eliminated by titrating arabinose induction. Bacteria were therefore cultivated in media supplemented with arabinose at the indicated concentrations, and expression levels were monitored by Western blotting as described below. Initial rates of proline uptake were measured using L-[U-<sup>14</sup>C]proline (GE Healthcare, Baie d'Urfé, QC) at 0.2 mM. All assays were conducted in triplicate, and all experiments were performed at least twice. Representative rates from single experiments are cited as the mean  $\pm$  standard deviation.

According to our standard procedure (38), an aliquot of a concentrated bacterial suspension in NaCl-free MOPS medium devoid of organic supplements is introduced into an assay medium of the desired osmolality, this mixture is aerated for 3 min, and radiolabeled proline is added to initiate the uptake reaction. To determine the impact of the aeration period on the rate of proline uptake, cells were added to assay buffer from which NaCl had been omitted, the mixture was incubated for 0, 1, 2, 3, 5, or 10 min at 25 °C, with shaking, and [<sup>14</sup>C]proline and NaCl were added to simultaneously impose an osmotic upshift and initiate proline uptake. Subsequent steps were performed as described previously (38). To determine the time course for the development of ProP activity following an osmotic upshift, NaCl was omitted from the assay buffer. Cell suspension was added to the assay buffer, and the mixture was incubated for 5 min at 25 °C, with shaking. NaCl was then added, and at various subsequent times, [<sup>14</sup>C]proline was added to initiate proline uptake. Subsequent steps were performed as previously described (38).

**Western Blotting.** Whole cell proteins were prepared for Western immunoblotting as described above (Transport Assays), and Western blotting was performed as described by Culham et al. (25) using the procedure of Towbin et al. (40). His-tagged proteins were detected with HRP-conjugated anti-pentaHis antibodies (Qiagen Inc., Mississauga, ON) and the ECL plus visualization system (GE Healthcare) according to the manufacturers' instructions.

**In Vivo Cross-Linking of ProPat.** The ability of dithiobis-(maleimidoethane) (DTME) to cross-link ProPat dimers *in vivo* was examined as described by Hillar et al. (27). Bacteria were cultivated in LB medium supplemented with sufficient D-arabinose to bring each ProPat variant to the level attained by ProPec\*-E480C without arabinose induction. ProPec-His<sub>6</sub>, used as an electrophoretic standard, was purified as described by Racher et al. (4).

**Protein Assays.** Protein concentrations were determined by the bicinchoninic acid assay (41) using the BCA kit from Pierce (Rockford, IL) with bovine serum albumin as the standard.

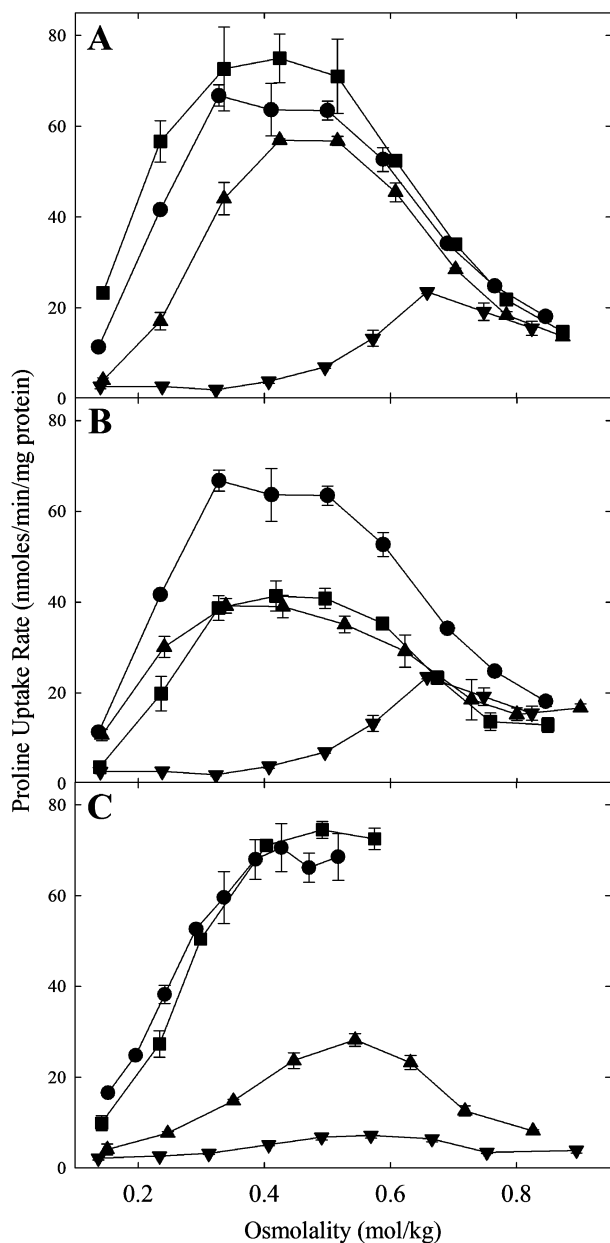


FIGURE 3: Impacts of mutations on the osmotic activation of ProP. Bacteria expressing ProPEc, ProPA, or a variant of either transporter were cultivated in NaCl-free MOPS medium (0.15 mol/kg), and initial rates of proline uptake were determined as described in Experimental Procedures using assay media adjusted to the indicated osmolalities with NaCl. The variants were (A) ProPEc (●), ProPEc-D475A (■), ProPEc-D478A (▲), and ProPEc-R488I (▼), (B) ProPEc (●), ProPEc-D475A/D478A (■), ProPEc-D475A/D476A/D478A (▲), and ProPEc-R488I (▼), and (C) ProPA (●), ProPA-R505I (▲), and ProPA-K498I/R505I (▼).

## RESULTS

**Impacts of Replacements D475A, D476A, and D478A on the Osmotic Activation of ProPEc.** The ProPEc coiled coil may be antiparallel because Arg 488 forms salt bridges with Asp 475 and Asp 478, and an Arg–Arg pair in the hydrophobic core would be destabilizing (Figure 1B) (18). As shown previously (25), mutation R488I profoundly altered the dependence of ProPEc activity on osmolality (Figure 3A). To determine how eliminating only the salt bridges would perturb activity, Asp 475 and Asp 478 were replaced with Ala, singly and in combinations. As expected, these muta-

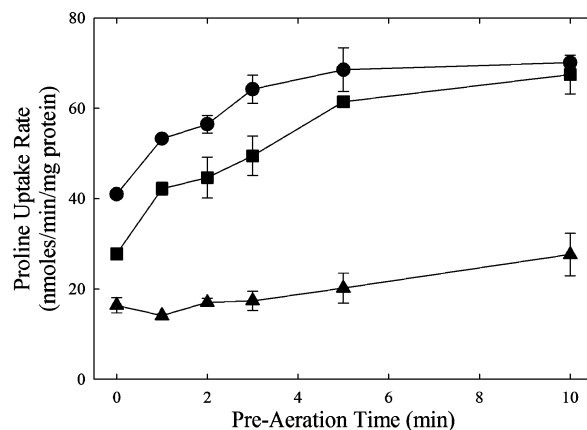


FIGURE 4: Pre-aeration period affects ProPEc activity after a subsequent osmotic upshift. Bacteria expressing ProPEc were cultivated in NaCl-free MOPS medium (0.15 mol/kg), and initial rates of proline uptake were determined after various pre-aeration periods as described in Experimental Procedures. Assay media were adjusted to 0.46 (●), 0.52 (■), or 0.89 mol/kg (▲) with NaCl as [ $^{14}$ C]proline was added to initiate the uptake assay at the indicated times after bacteria were diluted into the unadjusted transport assay mixture.

tions altered the osmotic activation profile of the transporter much less profoundly than did mutation R488I. Additional mutation D476A had no further effect (Figure 3B).

The initial rate of proline uptake via ProPEc increases over time after an osmotic upshift and is then sustained indefinitely (6, 25), whereas activation of ProPEc-R488I is transient (25). We refined our transport assay protocol before determining the impacts of additional mutations on this activation time course. Previous measurements indicated a longer half-time for ProPEc activation in cells [1 min (6)] than in proteoliposomes [ $<20$  s (4)]. Concentrated *E. coli* suspensions rapidly consume available oxygen, and osmotic upshifts inhibit respiration (42). Oxygen uptake measurements confirmed that respiration resumed slowly after *E. coli* cells were diluted from concentrated suspensions into our assay mixture (43). When cells were pre-aerated before NaCl and proline were added to simultaneously adjust the osmolality and initiate uptake, the measured proline uptake rate increased with pre-aeration time and the period to reach the maximum rate increased with osmolality (Figure 4). The assay protocol was therefore revised to ensure that cells were actively respiring before assays were initiated.

With a 5 min pre-aeration period, both ProPEc and ProPEc-R488I attained maximal activities within 1 min of an osmotic upshift (Figure 5). The activation time course was too rapid to be delineated by our transport assay, and it was undoubtedly influenced by effects of osmolality on both respiration and the transporter. However, the distinction between sustained activation of ProPEc and transient activation of ProPEc-R488I remained clear. Analogous measurements showed that activation of ProPEc-D475A/D478A was also sustained (Figure 5). Thus, eliminating the salt bridges of Arg 488 with Asp 475 and Asp 478 had weaker effects on ProPEc than simultaneously eliminating those salt bridges and increasing the hydrophobicity of the coiled-coil core, which occurs with replacement R488I (Table 2).

**Impacts of Replacements K498I and R505I on the Osmotic Activation of ProPA.** We turned to ProPA to further explore structure–function correlations for ProP. Tsatskis et al. (11)



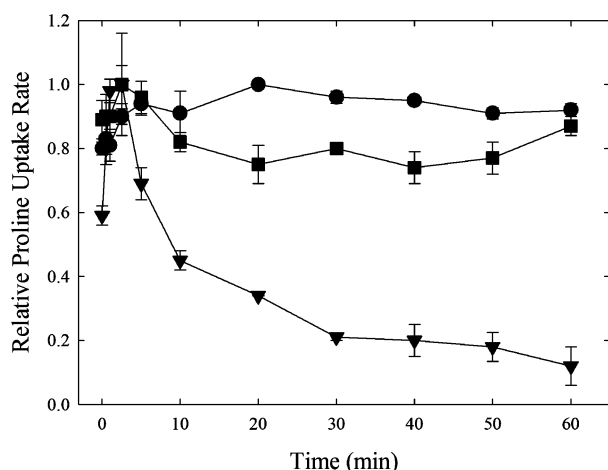


FIGURE 5: Impacts of mutations on the activation time course of ProPEc. Bacteria expressing ProPEc (●) or variant ProPEc-D475A/D478A (■) or ProPEc-R488I (▼) were cultivated in NaCl-free MOPS medium (0.15 mol/kg), and initial rates of proline uptake were determined as a function of time after an osmotic upshift as described in Experimental Procedures. Assay media were adjusted to the following osmolalities with NaCl: 0.46 mol/kg for ProPEc and ProPEc-D475A/D478A and 0.68 mol/kg for ProPEc-R488I. Relative rates of proline uptake were calculated by dividing each rate by the maximum rate measured for the corresponding variant (nanomoles per minute per milligram of protein): 96.56 for ProPEc, 58.63 for ProPEc-D475A/D478A, and 17.91 for ProPEc-R488I.

showed that the relationship between proline uptake activity and osmolality for ProPA $t$  is analogous to that of ProPEc when both are expressed in *E. coli* (compare panels A and C of Figure 3). In addition, both transporters undergo sustained osmotic activation (compare Figures 5 and 6).

We compared the impacts of substitutions K498I and R505I, singly and in combination, on the osmolality dependence and osmotic activation kinetics of ProPA $t$ . ProPA $t$ -K498I was similar in properties to ProPA $t$ , though the activity of ProPA $t$ -K498I declined a little with time after an osmotic upshift [compare squares (ProPA $t$ -K498I) with circles (ProPA $t$ ) in Figures 3C and 6]. The impact of replacement R505I on the osmolality dependence of ProPA $t$  activity [in Figure 3C, compare triangles (R505I) with circles (WT)] was very similar to the impact of replacement R488I on the osmolality dependence of ProPEc activity [in Figure 3A, compare inverted triangles (R488I) with circles (WT)]. In both cases, the amplitude of osmotic activation decreased and a much higher osmolality was required to elicit that activation for the mutant than for the WT. However, like that of ProPA $t$ -K498I, the osmotic activation of ProPA $t$ -R505I declined only slightly with time after an osmotic upshift [in Figure 6, compare squares (ProPA $t$ -K498I) with triangles (ProPA $t$ -R505I)]. When replacements K498I and R505I were combined, the resulting transporter had minimal activity regardless of osmolality (Figure 3C, inverted triangles) or time after an osmotic upshift (Figure 6, inverted triangles). Induction of transporter expression with D-arabinose at levels up to 13.3 mM failed to enhance this activity (data not shown).

The experiments described above were performed with untagged ProPA $t$  and its variants. To determine whether the measured activities (Figures 3C and 6) were influenced by variable transporter expression levels, a six-His tag was added to the C-terminus of each transporter and their activities and expression levels were estimated. ProPA $t$ -K498I/R505I-His<sub>6</sub>

was expressed at a lower level than the other variants when all four were induced by adding 0.4 mM arabinose to the culture medium (data not shown). However, the activity of ProPA $t$ -K498I/R505I-His<sub>6</sub> remained low even when 4 mM D-arabinose was used, and its expression became comparable to that of the other variants (Figure 7). Thus, this low activity was a property of the transporter itself, not a consequence of its expression level.

**Impacts of Replacements K498I and R505I on Stability and Orientation for Peptide Replicas of the ProPA $t$  C-Terminal Domain.** Multiple factors could influence the relative stabilities of the antiparallel ProPEc and ProPA $t$  coiled coils. The interactions in the extra heptad of the ProPA $t$  coiled coil might confer higher stability (Figure 2A,C). Arg 505 and Lys 498 of ProPA $t$  are at *a* positions and may form interchain salt bridges with two residues (Glu 485 and Asp 488) and one residue (Glu 495), respectively. The salt bridges would stabilize the coiled coil and favor the antiparallel orientation. However, the two charged residues limit the continuous arrays of hydrophobic residues at core *a* and *d* positions to only five per chain in both sequences. Furthermore, only two consecutive pairs of hydrophobic residues are paired across the coiled-coil core in ProPEc (Figure 2A), and none of the hydrophobic pairs are consecutive in ProPA $t$  (Figure 2C). On balance, the coiled coil of ProPA $t$  was predicted to be more stable than that of ProPEc. A ProPA $t$  variant with Ile replacing both Lys 498 and Arg 505 was predicted to form highly stable, parallel coiled coils with nine continuous pairs of large hydrophobes in core positions (Figure 2D).

Circular dichroism (CD) spectroscopy was used to measure the impact of the K498I and R505I replacements (singly and in combination) on the helical content of each peptide (Figure 8A) and its stability (Figure 8B). Helical content in benign solvent ( $\Theta_{222}$  for each peptide as a percent of  $\Theta_{222}$  for the fully folded helical peptide ProPA $t$ -K498I/R505I) and ellipticity ratio ( $\Theta_{222}/\Theta_{208}$ ) were used to assess coiled-coil formation (44) (Table 2). As predicted, the peptide with double replacement K498I/R404I was a fully folded coiled coil (100%  $\alpha$ -helical) with  $\Theta_{222}/\Theta_{208}$  greater than 1.0, but the WT peptide was moderately helical (80% relative to ProPA $t$ -K498I/R505I), with  $\Theta_{222}/\Theta_{208}$  slightly less than 1.0. Like ProPA $t$ -K498I/R505I, peptide ProPA $t$ -K498I had almost the maximum helical content and an ellipticity ratio greater than 1.0. In contrast, peptide ProPA $t$ -R505I had a much lower helical content, with spectral minima shifted to lower wavelengths and an ellipticity ratio of  $<0.9$ , indicative of more randomness. CD spectroscopy was also used to record the thermal denaturation profiles of the peptides (Figure 8B) and determine the temperature at the midpoint of each thermal transition ( $T_m$ ) (Table 2). As expected, the WT ProPA $t$  coiled coil ( $T_m = 45.5^\circ\text{C}$ ) was significantly more stable than the WT ProPEc coiled coil [ $T_m = 28^\circ\text{C}$  (26)]. The properties of the ProPA $t$  peptides reflected the anticipated thermal destabilization due to the R505I substitution and the stabilizing effect of the K498I substitution. Surprisingly, the thermal stability of double replacement peptide ProPA $t$ -K498I/R505I was similar to that of single replacement peptide ProPA $t$ -K498I, despite introduction of the destabilizing R505I substitution.

These results showed that the contributions of the K498I and R505I substitutions to coiled-coil structure and stability

Table 2: Properties of Peptides and ProP Variants

ProP variant <sup>a</sup>	continuous paired hydrophobes in the coiled-coil core <sup>b</sup>		peptide properties <sup>c</sup>				transporter properties <sup>d</sup>				
							amplitude			cross-linked cysteines	
	antiparallel	parallel	[Θ] <sub>222</sub> (% helix)	[Θ] <sub>222</sub> /[Θ] <sub>208</sub>	T <sub>m</sub> (°C)	threshold				duration	central
ProPEc	2	5	−14400 <sup>e</sup> (39%)	0.86 <sup>e</sup>	28 <sup>e</sup>	normal	normal	sustained	yes	no	
ProPEc-R488I	6	7	−8660 <sup>e</sup> (24%)	0.66 <sup>e</sup>	NT <sup>f</sup>	reduced	markedly elevated	transient	yes	yes	
ProPEc-D475A/D478A <sup>e</sup>	2	5	NT <sup>f</sup>	NT <sup>f</sup>	NT <sup>f</sup>	reduced	slightly elevated	sustained	NT <sup>f</sup>	NT <sup>f</sup>	
ProPA <sub>t</sub>	1	5	−25900 (80%)	0.97	45.5	normal	normal	sustained	yes	no	
ProPA <sub>t</sub> -K498I	4	7	−31300 (97%)	1.01	63.5	normal	normal	sustained	NT <sup>f</sup>	NT <sup>f</sup>	
ProPA <sub>t</sub> -R505I	3	5	−16000 (50%)	0.88	<10	reduced	markedly elevated	sustained	NT <sup>f</sup>	NT <sup>f</sup>	
ProPA <sub>t</sub> -K498I/R505I	8	9	−32200 (100%)	1.05	64.0	inactive	NA <sup>g</sup>	NA	yes	yes	

<sup>a</sup> ProPEc and ProPA<sub>t</sub> are the ProP orthologues from *E. coli* and *A. tumefaciens*, respectively. See Figure 1C for relevant amino acid sequences.

<sup>b</sup> Maximum number of continuous pairs of hydrophobic residues at coiled-coil core positions *a* and *d*. For example, the WT *E. coli* coiled coil has one run of two continuous pairs plus two single pairs of hydrophobic residues. <sup>c</sup> [Θ]<sub>222</sub> and [Θ]<sub>208</sub> are ellipticities at 10 °C. For the ProPA<sub>t</sub> peptides, the % helix is the helicity of each peptide in benign buffer as a percentage of the helicity of the fully folded peptide ProPA<sub>t</sub>-K498I/R505I under benign conditions. T<sub>m</sub> is the temperature at which a 50% decrease in folding occurred. <sup>d</sup> The osmotic activation profiles (Figures 3, 5, and 6) are described by specifying their amplitude (the maximum activity attained), the threshold for osmotic activation (the osmolality at which transporter activity begins to rise), and the duration of activity (whether it remains 1 hour or more after an osmotic upshift). For ProPA<sub>t</sub>, cross-linking of Cys residues introduced at the center of the coiled-coil sequence (central) or near the C-terminus (peripheral) is illustrated in Figure 10. Cross-linking of ProPEc was reported by Hillar et al. (27). <sup>e</sup> Properties of the wild-type and R488I ProPEc peptides were reported previously (25, 26). The reported T<sub>m</sub> of 28 °C was based on analysis of the ProPEc peptide at a concentration of 95 μM at pH 7.5. <sup>f</sup> Not tested. <sup>g</sup> Not applicable.

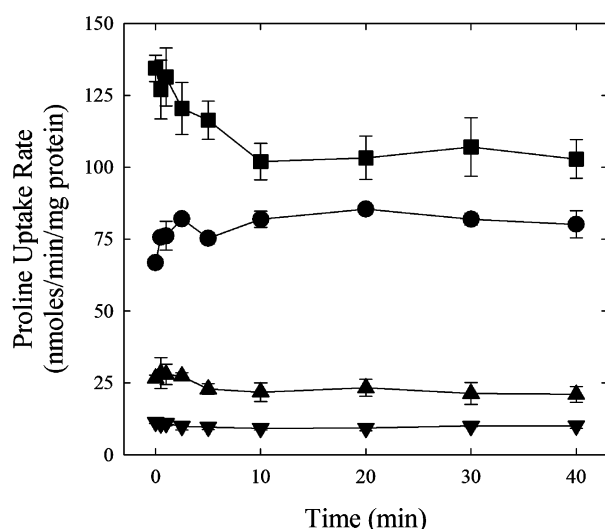


FIGURE 6: Impacts of mutations on the activation time course of ProPA<sub>t</sub>. Bacteria expressing ProPA<sub>t</sub> (●) or variant ProPA<sub>t</sub>-K498I (■), ProPA<sub>t</sub>-R505I (▲), or ProPA<sub>t</sub>-K498I/R505I (▼) were cultivated in NaCl-free, arabinose-supplemented (0.4 mM) MOPS medium (0.15 mol/kg), and initial rates of proline uptake were determined as a function of time after an osmotic upshift as described in Experimental Procedures. After pre-aeration, assay media were adjusted with NaCl to an osmolality of 0.51 mol/kg.

were neither equal nor additive. To determine whether coiled-coil orientation changes may contribute to differences in helical content and stability among these peptides, we determined the thermodynamically preferred orientation for the coiled coil formed by each peptide variant. Two variants of each sequence were designed so that covalently cross-linked, parallel homodimers and antiparallel heterodimers could be differentiated by RPC. Flexible Trp-Gly-Gly-Cys and Gly-Gly-Cys linkers were added to the N- and C-termini, respectively, of each longer peptide, and a Gly-Gly-Cys linker was added only to the C-terminus of each shorter peptide (Table 3). A differential Cys-protection scheme with two different thiol-protecting groups was used during

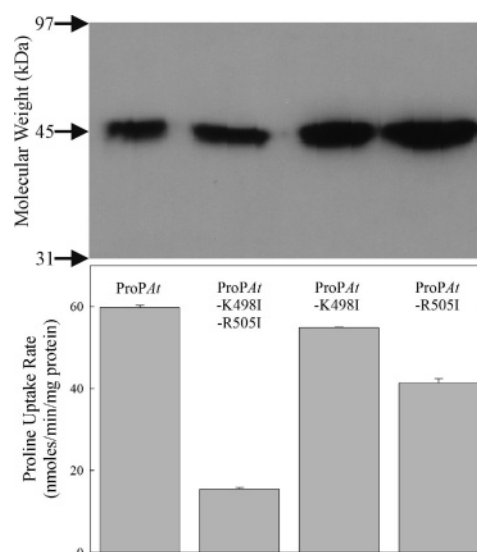


FIGURE 7: Expression levels of His-tagged ProPA<sub>t</sub> variants. The expression levels (top) and activities (bottom) of the His-tagged ProPA<sub>t</sub> variants were measured as described in Experimental Procedures. Bacteria were cultivated in NaCl-free MOPS medium containing 0.4 mM arabinose (ProPA<sub>t</sub>-His<sub>6</sub>, ProPA<sub>t</sub>-K498I-His<sub>6</sub>, and ProPA<sub>t</sub>-R505I-His<sub>6</sub>) or 4 mM arabinose (ProPA<sub>t</sub>-K498I/R505I-His<sub>6</sub>). Initial rates of proline uptake were measured in MOPS medium supplemented with 0.2 M NaCl (0.56 mol/kg). Cell extracts (5 μg of protein) were separated by SDS-PAGE, and His-tagged ProPA<sub>t</sub> variants were detected by Western blotting. A replicate gel stained with Gelcode Blue showed equivalent levels of other proteins among the four samples.

synthesis (see Experimental Procedures for details) so that each peptide could form only homo-stranded parallel coiled coils, cross-linked at the same termini and with partners of the same length.

First, each shorter peptide was oxidized, forming C-terminally disulfide-linked homo-stranded molecules. Next, each longer peptide was oxidized to form N-terminally disulfide-linked homo-stranded molecules. Equimolar quantities of these parallel homo-stranded molecules were then



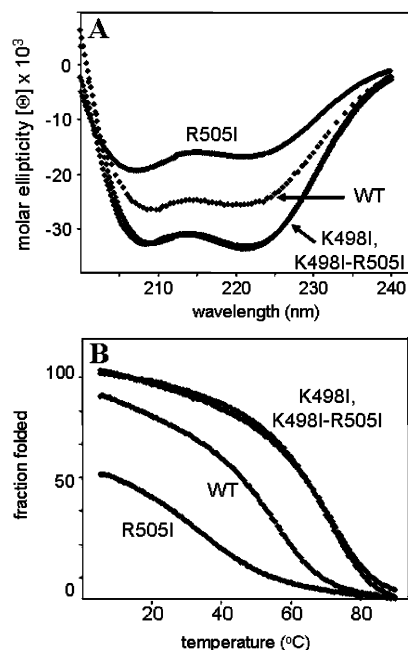


FIGURE 8: Secondary structures and stabilities of ProPA<sub>t</sub> peptides. Peptide sequences (short versions) are listed in Table 3. CD spectra were determined under reducing conditions in benign solvent [100 mM KCl, 50 mM KPO<sub>4</sub> (pH 7.4), and 0.2 mM DTT]. Mean residue molar ellipticity has units of degrees per square centimeter per decimole. (A) Circular dichroism (CD) spectra of the reduced ProPA<sub>t</sub> peptides. (B) Thermal stabilities of the reduced ProPA<sub>t</sub> peptides monitored at 222 nm in benign solvent (converted to fraction folded relative to the most helical analogue, K498I/R505I).

mixed in a redox buffer containing equimolar reduced and oxidized glutathione (pH 8.0) to promote disulfide bond exchange and allow selection of the most thermodynamically stable peptide orientation. In this system, starting parallel homo-stranded molecules comprised of peptides with equal lengths may be maintained or may undergo disulfide exchange to form antiparallel hetero-stranded molecules comprised of one short and one long peptide. Figure 9 shows that, at equilibrium, peptides ProPA<sub>t</sub> and ProPA<sub>t</sub>-K498I had switched to antiparallel hetero-stranded coiled coils of different lengths. These coiled coils with the antiparallel orientation were the more stable and preferred, because little of the starting, parallel homo-stranded molecules remained. In contrast, both parallel homo-stranded molecules (starting material) and antiparallel hetero-stranded molecules (after equilibration) were observed for ProPA<sub>t</sub>-R505I, hinting that there was little stability preference for either orientation. Given its low helical content (50%) and poor thermal stability ( $T_m < 10$  °C), ProPA<sub>t</sub>-R505I may not have formed a coiled coil of either orientation at room temperature. In contrast, even after being mixed for 4 h in redox buffer, most of peptide ProPA<sub>t</sub>-K498I/R505I remained homo-stranded. Thus, the elevated thermal stability of this peptide may be conferred by the double Ile replacements, and the resultant continuous hydrophobic core maintained this fully folded coiled coil in the very stable parallel conformation rather than the antiparallel orientation preferred by ProPA<sub>t</sub> and ProPA<sub>t</sub>-K498I.

**Cross-Linking Confirms Predicted Impacts of Replacements K498I and R505I on Coiled-coil Orientation for ProPA<sub>t</sub> In Vivo.** Cross-linking was used to determine whether ProPA<sub>t</sub> could form dimers *in vivo* and whether the relative orientations of ProPA<sub>t</sub> C-termini were affected by replace-

ments K498I and R505I. Dithiobis(maleimidoethane) (DTME) is a bifunctional thiol reagent with a cross-link length of approximately 1.3 nm and a cleavable disulfide. In previous studies based on a ProPEc variant lacking all four native Cys residues, position-specific DTME cross-linking of ProPEc was shown to occur *in vivo* (10). Cysteines are present at the same four positions in ProPA<sub>t</sub> and ProPEc, and evidence suggests that the ProPEc Cys residues are in the protein core (9). As expected, DTME did not cross-link ProPA<sub>t</sub>-His<sub>6</sub> (data not shown). Residues Q497 and L508 were separately replaced with Cys in the backgrounds of ProPA<sub>t</sub>-His<sub>6</sub> and ProPA<sub>t</sub>-K498I/R505I-His<sub>6</sub>. The Cys substitution variants retained transport activity (data not shown). Like previously cross-linked residue 480C of ProPEc (10), residue 497 of ProPA<sub>t</sub> is at a heptad *g* position, at the midpoint of the coiled-coil sequence (Figure 2C,D). DTME was expected to cross-link the ProPA<sub>t</sub>-Q497C C-termini if they formed coiled coils with the indicated registers, whether their orientation was antiparallel (Figure 2C) or parallel (Figure 2D). ProPA<sub>t</sub> residue 508 is at a heptad *d* position, selected because insertion of a disulfide bond at the *d* position in a model two-stranded coiled coil did not perturb the structure and contributed to coiled-coil stability (45). The 508C residues of an antiparallel ProPA<sub>t</sub> coiled coil with the register illustrated in Figure 2C would be too far apart for DTME cross-linking, whereas those in the parallel coiled coil illustrated in Figure 2D would be close and may spontaneously form disulfide bridges.

DTME cross-linking of these ProPA<sub>t</sub> variants yielded the expected results (Figure 10). ProPA<sub>t</sub>-Q497C-His<sub>6</sub> migrated predominantly with an apparent molecular weight (MW) of approximately 45 kDa before DTME treatment (predicted MW of 56 kDa). Anomalous migration is characteristic of integral membrane proteins like ProP, as illustrated by the migration of the purified ProPEc-His<sub>6</sub> standard. A little protein with the dimer molecular weight of 90 kDa was present for each ProPA<sub>t</sub> variant without DTME treatment. However, substantial quantities of ProPA<sub>t</sub>-Q497C-His<sub>6</sub> migrated with apparent molecular weights of 45 kDa (monomer) and 90 kDa (dimer) after DTME treatment. DTME also increased the proportion of dimeric ProPA<sub>t</sub>-Q497C/K498I/R505I-His<sub>6</sub>, as expected (Figure 2D). ProPA<sub>t</sub>-L508C-His<sub>6</sub> was predominantly monomeric without or with DTME, as expected for distal 508C residues in proteins with an antiparallel coiled coil (Figure 2C). In contrast, ProPA<sub>t</sub>-K498I/R505I/L508C-His<sub>6</sub> was predominantly dimeric in the absence of DTME, and DTME treatment rendered some protein monomeric. This would be expected if this variant forms parallel coiled coils (Figure 2D), the 508C residues in its core spontaneously form disulfide bridges, and modification of a 508C residue with DTME sterically inhibits both dimerization and further cross-linking. A strongly antibody-reactive protein with an apparent MW of approximately 60 kDa was observed only after DTME treatment of cells expressing either K497C variant of ProPA<sub>t</sub> (asterisks). This could indicate cross-linking of ProPA<sub>t</sub>-Q497C to its own proteolytic fragment or a different *E. coli* protein.  $\beta$ -Mercaptoethanol [5% (v/v)] treatment eliminated the 90 and 60 kDa species, but not that with an apparent MW of 45 kDa (data not shown). Since no lower-MW species were observed with or without  $\beta$ -mercaptoethanol

Table 3: Peptide Nomenclature and Sequences of ProP<sub>At</sub> Peptides Used in This Study<sup>a</sup>

Peptide Name	Continuous Hydrophobic <i>a</i> and <i>d</i> Residues Per Peptide	Peptide Sequence
		<b>bcdefgabcdefgabcdefgabcdefgabcdefgabcde</b>
WT	5	QHIEKSVEEIDEE <b>LAKLEE</b> QKKILQTK <b>R</b> EGLVGRHPDLTGGC
K498I	7	QHIEKSVEEIDEE <b>LAKLEE</b> Q <b>I</b> KILQTK <b>R</b> EGLVGRHPDLTGGC
R505I	5	QHIEKSVEEIDEE <b>LAKLEE</b> QKKILQTK <b>I</b> EGLVGRHPDLTGGC
K498I-R505I	9	QHIEKSVEEIDEE <b>LAKLEE</b> Q <b>I</b> KILQTK <b>I</b> EGLVGRHPDLTGGC
WT_L	5	WCGGQHIEKSVEEIDEE <b>LAKLEE</b> QKKILQTK <b>R</b> EGLVGRHPDLTGGC
K498I_L	7	WCGGQHIEKSVEEIDEE <b>LAKLEE</b> Q <b>I</b> KILQTK <b>R</b> EGLVGRHPDLTGGC
R505I_L	5	WCGGQHIEKSVEEIDEE <b>LAKLEE</b> QKKILQTK <b>I</b> EGLVGRHPDLTGGC
K498I-R505I_L	9	WCGGQHIEKSVEEIDEE <b>LAKLEE</b> Q <b>I</b> KILQTK <b>I</b> EGLVGRHPDLTGGC

<sup>a</sup> The WT peptide corresponds to residues 478–516 of ProP<sub>At</sub>. The heptad repeat, denoted as *abcdefg*, is shown above the peptide sequences with residues at positions *a* and *d* in the hydrophobic core bold and the sites of substitutions underlined. Substitutions K498I and R505I are at heptad *a* positions. Two versions of each peptide were synthesized, a shorter version with Gly-Gly-Cys linker at the C-terminus and a longer version (denoted *\_L*) with Trp-Cys-Gly-Gly at the N-terminus and Gly-Gly-Cys at the C-terminus (see Experimental Procedures).

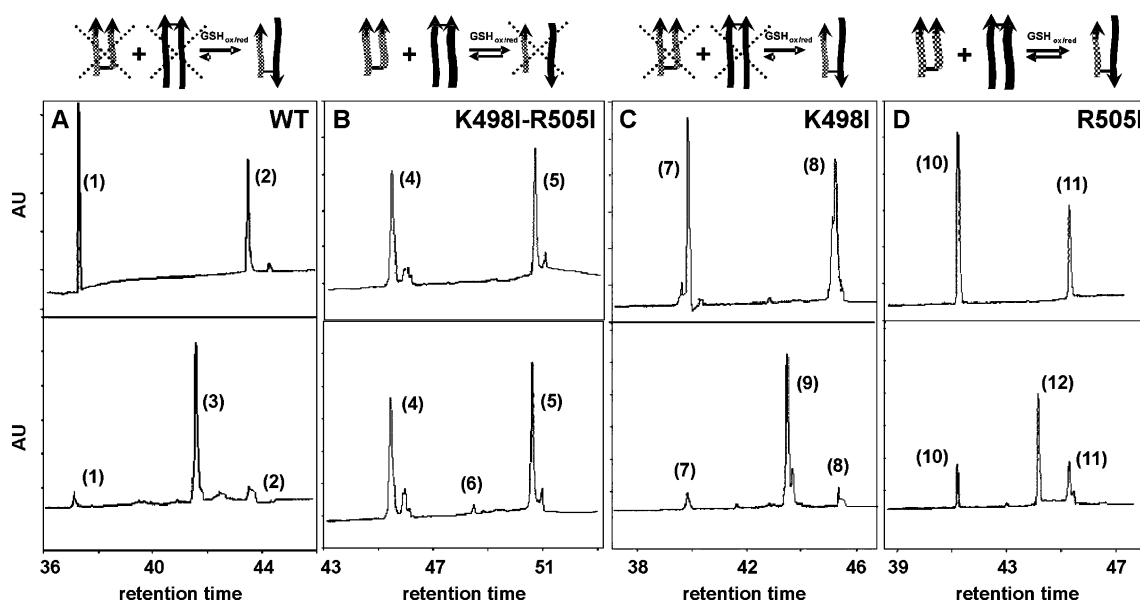


FIGURE 9: Impact of REDOX disulfide exchange on coiled-coil orientation for Cys-bridged ProP<sub>At</sub> peptides. Peptide sequences are listed in Table 3. Each panel shows a reversed-phase HPLC chromatogram of disulfide-linked ProP<sub>At</sub> peptides, both short and long versions. The short and long peptides were mixed and the data obtained before (top panels) and after (bottom panels) 4 h in glutathione-containing buffer as described in Experimental Procedures. The cartoons above the panels illustrate the reactions, Xs marking species that were poorly represented at equilibrium. (A) WT ProP<sub>At</sub> peptides [short (1) and long (2) versions]. The peak at a retention time of 42 min (3) showed the emergence of the antiparallel Cys-linked hetero-stranded coiled coil comprised of one short and one long peptide. (B) ProP<sub>At</sub>-K498I/R505I peptides [short (4) and long (5) versions]. The peak at a retention time of 48.5 min (6) was small, showing little formation of antiparallel hetero-stranded molecules. (C) ProP<sub>At</sub>-K498I peptides [short (7) and long (8) versions]. The peak at 44 min (9) showed the emergence of the antiparallel Cys-linked hetero-stranded coiled coil comprised of one short and one long peptide. (D) ProP<sub>At</sub>-R505I peptides [short (10) and long (11) versions]. The peak at 44 min (12) showed the emergence of the antiparallel Cys-linked hetero-stranded coiled coil comprised of one short and one long peptide, but some starting material also remained [parallel homo-stranded molecules (11 and 12)].

treatment, no proteolytic degradation of these ProP<sub>At</sub> variants was evident.

## DISCUSSION

The coiled-coil sequence of ProP<sub>At</sub> is longer by one heptad than the coiled-coil sequence of ProP<sub>Ec</sub>. Sequence alignments suggested that the antiparallel orientations of both coiled coils would be stabilized by specific ionic interactions involving charged residues in the hydrophobic core. As expected, a peptide corresponding to the ProP<sub>At</sub> sequence formed a more stable coiled coil than a peptide corresponding to the ProP<sub>Ec</sub> sequence [*T<sub>m</sub>* = 45 and 28 °C, respectively

(Figure 8 and Table 2)]. We tested the prediction that the ProP<sub>At</sub> coiled coil is antiparallel and examined the impact of replacing the core basic residues with Ile on its secondary structure, stability, orientation, and function.

Redox analysis confirmed that the WT ProP<sub>At</sub> peptide formed antiparallel coiled coils at equilibrium (Figure 9). Peptide ProP<sub>At</sub>-K498I formed an even more stable, fully folded  $\alpha$ -helical coiled coil (12) that retained the antiparallel orientation (Figures 8 and 9 and Table 2) (13). Thus, neither coiled-coil formation nor antiparallel orientation required electrostatic stabilization by Lys 498. Replacement of that residue not only was tolerated but also enhanced the helicity

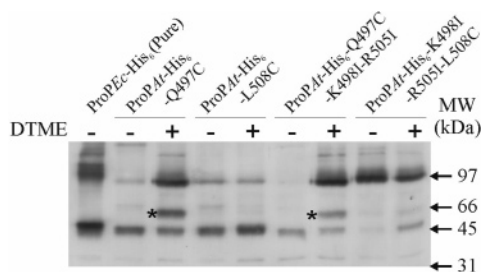


FIGURE 10: DTME-mediated *in vivo* cross-linking of ProPA variants. Bacteria expressing ProPA variants were cultivated in LB medium; proteins were cross-linked with DTME, and cell extracts were analyzed by SDS-PAGE and Western blotting as described in Experimental Procedures. D-Arabinose was added at 50  $\mu$ M to induce expression of ProPA $t$ -Q497C/K498I/R505I-His<sub>6</sub> and at 5  $\mu$ M to induce expression of the other proteins. Molecular weight markers with the indicated sizes (MW) and purified ProPEc-His<sub>6</sub> were used as standards. Monomeric and dimeric ProPA $t$  migrate with apparent molecular weights of approximately 40 and 90 kDa, respectively, in this system. Plus and minus signs denote the presence and absence of DTME, respectively. ProPA $t$  variants with replacement Q497C formed an unexpected species with an apparent molecular weight of approximately 60 kDa (asterisk; see text).

and stability of the coiled coil (Figure 8). In contrast, the helical secondary structure and stability of the ProPA $t$ -R505I variant were low, and it did not prefer either orientation (Figures 8 and 9 and Table 2). This suggested that R505, equivalent to R488 in *E. coli*, is a more important determinant of coiled-coil stability and antiparallel orientation than K498. Surprisingly, the peptides with the single replacement K498I and the double replacement K498I/R505I had similar, high stabilities (Figures 8 and 9 and Table 2). This apparent paradox was resolved by the observation that peptides ProPA $t$  and ProPA $t$ -K498I/R505I were in opposite orientations. ProPA $t$ -K498I/R505I had switched to the parallel orientation because a long, continuous hydrophobic core had been created and Arg residues were no longer paired in the hydrophobic core.

Recently, DTME cross-linking of introduced Cys residues showed that the C-termini of ProPEc dimers are antiparallel *in vivo*. Mutation R488I promoted cross-linking that would be facilitated by reorientation of the C-termini to a parallel alignment (27). Here we applied analogous tools to ProPA $t$ . DTME treatment increased the amount of dimer present for both ProPA $t$ -Q497C-His<sub>6</sub> and ProPA $t$ -Q497C/K498I/R505I-His<sub>6</sub> (Figure 10), showing the proximity of the C-termini in both protein dimers. DTME did not increase the amount of dimeric ProPA $t$ -L508C-His<sub>6</sub>; on the other hand, ProPA $t$ -K498I/R505I/L508C-His<sub>6</sub> in control samples was predominantly dimeric, and that proportion decreased slightly in DTME-treated cells (Figure 10). These observations support the view that antiparallel and parallel coiled coils are present in ProPA $t$  and ProPA $t$ -K498I/R505I, respectively. These data support the view that group A ProP orthologues are homodimers in which the C-termini form intermolecular, antiparallel coiled coils. However, the C-termini of ProPA $t$  can align in parallel when only Arg 505 is replaced with Ile, and stable parallel coiled coils can form when both Arg 505 and Lys 498 are replaced with Ile.

This information contributes to the following functional model for osmosensing and the osmotic adaptation of ProP. Group A (10) and B ProP orthologues are homodimers with interfaces that include TM XII residues. The C-termini of

group A orthologues can form intermolecular, antiparallel coiled coils (refs 10, 18, and 25–27 and this paper) that favor but are not essential for conformational changes associated with osmotic activation (11, 46). When bacteria are cultivated and maintained at low osmolality, the ProP C-termini may associate with the membrane surface, a different part of ProP, or a different protein. The full C-terminal domain [not just the coiled-coil-forming sequence (Figure 1C)] may be involved in such an interaction, and it would be preferred over homodimeric coiled-coil formation for group A orthologues. Homodimeric coiled-coil formation would be increasingly favored as cytoplasmic ionic strength and the degree of crowding increase with medium osmolality. Group A orthologues, with a coiled coil, would then be activated at a lower osmolality than group B orthologues, without a coiled coil (11, 25).

Recently, we showed that ProPEc and cardiolipin (CL) colocalize near the poles and septa of *E. coli* cells and the polar localization of ProPEc is CL-dependent (47). The CL content of *E. coli* and the osmolality required to activate ProPEc increase in parallel with growth medium osmolality (11). The osmolality required to activate ProPEc also increases with the proportion of anionic lipid (CL or phosphatidylglycerol) in proteoliposomes (T. Romantsov and J. M. Wood, unpublished data). These observations suggest that, *in vivo*, the C-terminal domain of ProPEc may interact with CL and this interaction may impair osmotic activation. Membrane (CL) surface association of ProPEc may compete with intermolecular coiled-coil formation.

This model is further supported by our studies of ProP variants with altered coiled coils. Homologous amino acid replacements R488I (in ProPEc) and R505I (in ProPA $t$ ) impair coiled-coil formation by peptide replicas (ref 25 and Figure 8) and elevate the osmolality required for osmotic activation of the intact transporters (Figure 3). Osmotic upshifts only transiently activate ProPEc-R488I (ref 25 and Figure 5), so it is inactive when bacteria are maintained at low osmolality or exposed to high-osmolality media for long periods. DTME cross-links the C-termini of ProPEc-R488I if Cys is introduced at position 473 or 480 because the C-termini of these dimeric transporters are in the same vicinity and this mutation destabilizes the antiparallel orientation (27). In addition, transitions to the active conformation may facilitate parallel alignment of the C-termini, locking this transporter in an inactive, osmolality-refractory state and facilitating cross-linking at both sites (10). No activation time course can be delineated for ProPA $t$ -K498I/R505I because it responds little to osmotic upshifts (Figures 3, 6, 7, and 10). Even at low osmolality this transporter forms stable, parallel coiled coils that can be visualized as disulfide-bridged two-stranded molecules when residue L508 is replaced with Cys (Figure 10). Hence, ProPA $t$ -K498I/R505I is always refractory to osmotic upshifts (Figures 3, 6, 7, and 10).

This switch between antiparallel and parallel orientations for the ProP C-termini illustrates the concept that coiled-coil domains not only are important in mediating assembly in large complexes but also may be important for dynamic subunit realignment. For example, coiled coils in the SNARE complex are known to align in either an antiparallel or a parallel orientation depending on cellular functions (48), and variants of GCN4 can populate both parallel and antiparallel



orientations depending on crystallographic conditions (49). In this study, peptides ProPA<sub>t</sub>-K498I and ProPA<sub>t</sub>-K498I/R505I formed equally stable coiled-coil dimers; however, transporter ProPA<sub>t</sub>-K498I was activated as osmolality increased, whereas transporter ProPA<sub>t</sub>-K498I/R505I was refractory to osmotic activation. This functional difference correlated with the fact that the C-termini within the transporter dimers were opposite in orientation. To date, most coiled-coil mutational switching investigations have been performed *in vitro* with emphasis on structural biology, protein stability, or amino acid interactions. Little or no *in vivo* evidence has been provided to demonstrate the interplay between coiled-coil alignment and function (21, 50, 51). This study highlights the relationship between *in vitro* structural studies and corresponding functional modifications in living cells, thus stressing the future possibility of designing coiled coils with specific structural and functional impact *in vivo*.

## ACKNOWLEDGMENT

We are grateful to Doreen E. Culham (University of Guelph) for purified ProPEc-His<sub>6</sub>, to Tanya Romantsov (University of Guelph) for help with experiments, and to Dziuleta Cepeniene (University of Colorado Denver, School of Medicine) for peptide synthesis.

## SUPPORTING INFORMATION AVAILABLE

Masses and oligomeric states of peptides corresponding to ProPA<sub>t</sub> sequences (Table 1S). This material is available free of charge via the Internet at <http://pubs.acs.org>.

## REFERENCES

- Wood, J. M. (1999) Osmosensing by Bacteria: Signals and Membrane-Based Sensors, *Microbiol. Mol. Biol. Rev.* 63, 230–262.
- Wood, J. M. (2006) Osmosensing by bacteria, *Sci. STKE* 357, pe43.
- Bolen, D. W. (2001) Protein stabilization by naturally occurring osmolytes, *Methods Mol. Biol.* 168, 17–36.
- Racher, K. I., Voegelé, R. T., Marshall, E. V., Culham, D. E., Wood, J. M., Jung, H., Bacon, M., Cairns, M. T., Ferguson, S. M., Liang, W.-J., Henderson, P. J. F., White, G., and Hallett, F. R. (1999) Purification and reconstitution of an osmosensor: Transporter ProP of *Escherichia coli* senses and responds to osmotic shifts, *Biochemistry* 38, 1676–1684.
- Culham, D. E., Lasby, B., Marangoni, A. G., Milner, J. L., Steer, B. A., van Nues, R. W., and Wood, J. M. (1993) Isolation and sequencing of *Escherichia coli* gene *proP* reveals unusual structural features of the osmoregulatory proline/betaine transporter, ProP, *J. Mol. Biol.* 229, 268–276.
- Milner, J. L., Grothe, S., and Wood, J. M. (1988) Proline porter II is activated by a hyperosmotic shift in both whole cells and membrane vesicles of *Escherichia coli* K12, *J. Biol. Chem.* 263, 14900–14905.
- MacMillan, S. V., Alexander, D. A., Culham, D. E., Kunte, H. J., Marshall, E. V., Rochon, D., and Wood, J. M. (1999) The ion coupling and organic substrate specificities of osmoregulatory transporter ProP in *Escherichia coli*, *Biochim. Biophys. Acta* 1420, 30–44.
- Culham, D. E., Hillar, A., Henderson, J., Ly, A., Vernikovska, Ya. I., Racher, K. I., Boggs, J. M., and Wood, J. M. (2003) Creation of a fully functional, cysteine-less variant of osmosensor and proton-osmoprotectant symporter ProP from *Escherichia coli* and its application to assess the transporter's membrane orientation, *Biochemistry* 42, 11815–11823.
- Wood, J. M., Culham, D. E., Hillar, A., Vernikovska, Ya. I., Liu, F., Boggs, J. M., and Keates, R. A. B. (2005) Structural model for the osmosensor, transporter, and osmoregulator ProP of *Escherichia coli*, *Biochemistry* 44, 5634–5646.
- Liu, F., Culham, D. E., Vernikovska, Ya. I., Keates, R. A. B., Boggs, J. M., and Wood, J. M. (2007) Structure and function of the XII<sup>th</sup> transmembrane segment in osmosensor and osmoprotectant transporter ProP of *Escherichia coli*, *Biochemistry* 46, 5647–5655.
- Tsatskis, Y., Khambati, J., Dobson, M., Bogdanov, M., Dowhan, W., and Wood, J. M. (2005) The osmotic activation of transporter ProP is tuned by both its C-terminal coiled-coil and osmotically induced changes in phospholipid composition, *J. Biol. Chem.* 280, 41387–41394.
- Wagschal, K., Tripet, B., Lavigne, P., Mant, C. T., and Hodges, R. S. (1999) The role of position a in determining the stability and oligomerization state of  $\alpha$ -helical coiled coils: 20 amino acid stability coefficients in the hydrophobic core of proteins, *Protein Sci.* 8, 2312–2329.
- Tripet, B. P., Wagschal, K., Lavigne, P., Mant, C. T., and Hodges, R. S. (2000) Effects of side-chain characteristics on stability and oligomerization state of a de novo-designed model coiled-coil: 20 amino acid substitutions in position “d”, *J. Mol. Biol.* 300, 377–402.
- Wagschal, K., Tripet, B., and Hodges, R. S. (1999) De novo design of a model peptide sequence to examine the effects of single amino acid substitutions in the hydrophobic core on both stability and oligomerization state of coiled-coils, *J. Mol. Biol.* 285, 785–803.
- Monera, O. D., Zhou, N. E., Lavigne, P., Kay, C. M., and Hodges, R. S. (1996) Formation of parallel and antiparallel coiled-coils controlled by the relative positions of alanine residues in the hydrophobic core, *J. Biol. Chem.* 271, 3995–4001.
- Monera, O. D., Zhou, N. E., Kay, C. M., and Hodges, R. S. (1993) Comparison of antiparallel and parallel two-stranded  $\alpha$ -helical coiled coils. Design, synthesis, and characterization, *J. Biol. Chem.* 268, 19218–19227.
- Arndt, K. M., Pelletier, J. N., Müller, K. M., Plückthun, A., and Alber, T. (2002) Comparison of *in vivo* selection and rational design of heterodimeric coiled coils, *Structure* 10, 1235–1248.
- Zoetewey, D. L., Tripet, B. P., Kutateladze, T. G., Overduin, M. J., Wood, J. M., and Hodges, R. S. (2003) Solution structure of the C-terminal antiparallel coiled-coil domain from *Escherichia coli* osmosensor ProP, *J. Mol. Biol.* 334, 1063–1076.
- McClain, D. L., Gurnon, D. G., and Oakley, M. G. (2002) Importance of potential interhelical salt-bridges involving interior residues for coiled-coil stability and quaternary structure, *J. Mol. Biol.* 324, 257–270.
- Oakley, M. G., and Kim, P. S. (1998) A buried polar interaction can direct the relative orientation of helices in a coiled coil, *Biochemistry* 37, 12603–12610.
- Woolfson, D. N. (2005) The design of coiled-coil structures and assemblies, *Adv. Protein Chem.* 70, 79–112.
- Schnarr, N. A., and Kennan, A. J. (2004) Strand orientation by steric matching: A designed antiparallel coiled-coil trimer, *J. Am. Chem. Soc.* 126, 14447–14451.
- Hill, R. B., and Degrad, W. F. (1998) Solution structure of  $\alpha_2D$ , native-like *de novo* designed protein, *J. Am. Chem. Soc.* 120, 1138–1145.
- Schafmeister, C. E., Laporte, S. L., Miercke, L. J. W., and Stroud, R. M. (1997) A designed four helix bundle protein with native-like structure, *Nat. Struct. Biol.* 4, 1039–1046.
- Culham, D. E., Tripet, B., Racher, K. I., Voegelé, R. T., Hodges, R. S., and Wood, J. M. (2000) The role of the carboxyl terminal  $\alpha$ -helical coiled-coil domain in osmosensing by transporter ProP of *Escherichia coli*, *J. Mol. Recognit.* 13, 1–14.
- Hillar, A., Tripet, B., Zoetewey, D., Wood, J. M., Hodges, R. S., and Boggs, J. M. (2003) Detection of  $\alpha$ -helical coiled-coil dimer formation by spin-labeled synthetic peptides: A model parallel coiled-coil peptide and the antiparallel coiled-coil formed by a replica of the ProP C-terminus, *Biochemistry* 42, 15170–15178.
- Hillar, A., Culham, D. E., Vernikovska, Ya. I., Wood, J. M., and Boggs, J. M. (2005) Formation of an antiparallel, intermolecular coiled-coil is associated with *in vivo* dimerization of osmosensor and osmoprotectant transporter ProP in *Escherichia coli*, *Biochemistry* 44, 10170–10180.
- Kwok, S. C., and Hodges, R. S. (2004) Stabilizing and destabilizing clusters in the hydrophobic core of long two-stranded  $\alpha$ -helical coiled-coils, *J. Biol. Chem.* 279, 21576–21588.
- Tripet, B., Cepeniene, D., Kovacs, J. M., Mant, C. T., Krokshin, O. V., and Hodges, R. S. (2007) Requirements for prediction of peptide retention time in reversed-phase high-performance liquid chromatography: Hydrophilicity/hydrophobicity of side-chains at

- the N- and C-termini of peptides are dramatically affected by the end-groups and location, *J. Chromatogr., A* **1141**, 212–225.
30. Kwok, S. C., and Hodges, R. S. (2003) Clustering of large hydrophobes in the hydrophobic core of two-stranded  $\alpha$ -helical coiled-coils controls protein folding and stability, *J. Biol. Chem.* **278**, 35248–35254.
  31. Miller, J. H. (1972) *Experiments in Molecular Genetics*, Cold Spring Harbor Laboratory Press, Plainview, NY.
  32. Neidhardt, F. C., Bloch, P. L., and Smith, D. F. (1974) Culture medium for enterobacteria, *J. Bacteriol.* **119**, 736–747.
  33. Guzman, L.-M., Belin, D., Carson, M. J., and Beckwith, J. (1995) Tight regulation, modulation, and high-level expression by vectors containing the arabinose P<sub>BAD</sub> promoter, *J. Bacteriol.* **177**, 4121–4130.
  34. Sambrook, J., and Russell, D. W. (2001) *Molecular Cloning: A Laboratory Manual*, Cold Spring Harbor Laboratory Press, Plainview, NY.
  35. Bayliss, C., Lasby, B., Wood, J. M., Lifshitz, R., and Brown, G. L. (1993) Mutant derivatives of *Pseudomonas putida* GR12-2R3 defective in nutrient utilization or cell surface structures show reduced ability to promote canola root elongation, *Can. J. Microbiol.* **39**, 1111–1119.
  36. Brown, E. D., and Wood, J. M. (1992) Redesigned purification yields a fully functional PutA protein dimer from *Escherichia coli*, *J. Biol. Chem.* **267**, 13086–13092.
  37. Hanahan, D. (1983) Studies on transformation of *Escherichia coli* with plasmids, *J. Mol. Biol.* **166**, 557–569.
  38. Culham, D. E., Henderson, J., Crane, R. A., and Wood, J. M. (2003) Osmosensor ProP of *Escherichia coli* responds to the concentration, chemistry and molecular size of osmolytes in the proteoliposome lumen, *Biochemistry* **42**, 410–420.
  39. Racher, K. I., Culham, D. E., and Wood, J. M. (2001) Requirements for osmosensing and osmotic activation of transporter ProP from *Escherichia coli*, *Biochemistry* **40**, 7324–7333.
  40. Towbin, H., Staehelin, T., and Gordon, J. (1979) Electrophoretic transfer of proteins from polyacrylamide gels to nitrocellulose sheets: Procedure and some applications, *Proc. Natl. Acad. Sci. U.S.A.* **76**, 4350–4354.
  41. Smith, P. K., Krohn, R. I., Hermanson, G. T., Mallia, A. K., Gartner, F. H., Provenzano, M. D., Fujimoto, E. K., Goeke, N. M., Olson, B. J., and Klenk, D. C. (1985) Measurement of protein using bicinchoninic acid, *Anal. Biochem.* **150**, 76–85.
  42. Meury, J. (1994) Immediate and transient inhibition of the respiration of *Escherichia coli* under hyperosmotic shock, *FEMS Microbiol. Lett.* **121**, 281–286.
  43. Tsatskis, Y. (2005) The role of the C-terminal coiled-coil domain in osmosensing, osmotic activation and adaptation of *Escherichia coli* transporter ProP, M.Sc. Thesis, University of Guelph, Guelph, ON.
  44. Sonnichsen, F. D., Van Eyck, J. E., Hodges, R. S., and Sykes, B. D. (1992) Effect of trifluoroethanol on protein secondary structure: An NMR and CD study using a synthetic actin peptide, *Biochemistry* **31**, 8790–8798.
  45. Zhou, N. E., Kay, C. M., and Hodges, R. S. (1993) Disulfide bond contribution to protein stability: Positional effects of substitution in the hydrophobic core of the two-stranded  $\alpha$ -helical coiled-coil, *Biochemistry* **32**, 3178–3187.
  46. Peter, H., Weil, B., Burkovski, A., Krämer, R., and Morbach, S. (1998) *Corynebacterium glutamicum* is equipped with four secondary carriers for compatible solutes: Identification, sequencing, and characterisation of the proline/ectoine uptake system ProP and the ectoine/proline/glycine betaine carrier EctP, *J. Bacteriol.* **180**, 6005–6012.
  47. Romantsov, T., Helbig, S., Culham, D. E., Gill, C., Stalker, L., and Wood, J. M. (2007) Cardiolipin promotes polar localization of osmosensory transporter ProP in *Escherichia coli*, *Mol. Microbiol.* **64**, 1455–1465.
  48. Weninger, K., Bowen, M. E., Chu, S., and Brunger, A. T. (2003) Single-molecular studies of SNARE complex assembly reveal parallel and antiparallel configurations, *Proc. Natl. Acad. Sci. U.S.A.* **100**, 14800–14805.
  49. Maneesh, K. Y., Leman, L. J., Price, D. J., Brooks, C. L., Stout, C. D., and Ghadiri, M. R. (2006) Coiled-coils at the edge of conformational heterogeneity. Structural analyses of parallel and antiparallel homotetrameric coiled coils reveal configurational sensitivity to a single solvent-exposed amino acid substitution, *Biochemistry* **45**, 4463–4473.
  50. Lupas, A. (1996) Coiled coils: New structures and new functions, *Trends Biochem. Sci.* **21**, 375–382.
  51. Burkhard, P., Strelkov, S. V., and Stetefeld, J. (2001) Coiled-coils: A highly versatile protein folding motif, *Trends Cell Biol.* **11**, 82–88.
  52. Guex, N., and Peitsch, M. C. (1997) SWISS-MODEL and the Swiss-PdbViewer: An environment for comparative protein modeling, *Electrophoresis* **18**, 2714–2723.
  53. Schnell, J. R., Zhou, G. P., Zweckstetter, M., Rigby, A. C., and Chou, J. J. (2005) Rapid and accurate structure determination of coiled-coil domains using NMR dipolar couplings: Application to cGMP-dependent protein kinase I $\alpha$ , *Protein Sci.* **14**, 2421–2428.

BI7018173